# Climatic Variability of Near-Surface Turbulent Kinetic Energy over the United States: Implications for Fire-Weather Predictions

WARREN E. HEILMAN AND XINDI BIAN

*U.S. Department of Agriculture Forest Service Northern Research Station, East Lansing, Michigan*

## ABSTRACT

Recent research suggests that high levels of ambient near-surface atmospheric turbulence are often associated with rapid and sometimes erratic wildland fire spread that may eventually lead to large burn areas. Previous research has also examined the feasibility of using near-surface atmospheric turbulent kinetic energy ($TKE_s$) alone or in combination with the Haines index (HI) as an additional indicator of anomalous atmospheric conditions conducive to erratic or extreme fire behavior. However, the application of $TKE_s$-based indices for operational fire-weather predictions in the United States on a regional or national basis first requires a climatic assessment of the spatial and temporal patterns of the indices that can then be used for testing their operational effectiveness. This study provides an initial examination of some of the spatial and temporal variability patterns across the United States of $TKE_s$ and the product of HI and $TKE_s$ ($HITKE_s$) using data from the North American Regional Reanalysis dataset covering the 1979–2008 period. The analyses suggest that there are regional differences in the behavior of these indices and that regionally dependent threshold values for $TKE_s$ and $HITKE_s$ may be needed for their potential use as operational indicators of anomalous atmospheric turbulence conditions conducive to erratic fire behavior. The analyses also indicate that broad areas within the northeastern, southeastern, and southwestern regions of the United States have experienced statistically significant positive trends in $TKE_s$ and $HITKE_s$ values over the 1979–2008 period, with the most substantial increases in values occurring over the 1994–2008 period.

## 1. Introduction

The fundamental properties of atmospheric turbulence and the effects of forest vegetation, topography, and other land surface conditions on the generation, diffusion, and dissipation of atmospheric turbulence have been extensively studied and reported in the literature over the last 50 years (e.g., Deardorff 1974; Mellor and Yamada 1982; Meyers and Baldocchi 1991; Inall et al. 2005; Weigel et al. 2007; Park et al. 2012). These and many other studies have increased our basic understanding of atmospheric turbulence and its importance in land–water–atmosphere interactions, which play such a critical role in the evolution of the atmospheric boundary layer. In recent years, there has been an additional emphasis placed on studying the role of atmospheric turbulence in affecting wildland fire behavior,

some of which is described in the syntheses of fire–atmosphere interaction studies presented by Werth et al. (2011) and Potter (2012a,b). The emphasis is due in part to the many high profile wildland fires that have occurred in the United States over the last decade, the advances in mesoscale, large-eddy simulation and coupled fire–atmosphere modeling, and the advances in in situ and remote sensing turbulence monitoring capabilities within fire environments. A brief review of those studies is provided below.

In the area of atmospheric modeling as it relates to fire–atmosphere interactions, several noteworthy studies have been carried out that advance our understanding of turbulence impacts on fire behavior. Numerical simulations of wildland fire spread performed by Clark et al. (2004) using a nonhydrostatic mesoscale model coupled with fire spread algorithms found in the "BEHAVE" system (Rothermel 1972; Andrews 1986) showed that perturbations in the wind field (i.e., turbulent flow) along a fire line can lead to local perturbations in fire spread rates. This same coupled modeling system was used by Coen (2005) in simulations of the 2002 Big Elk

*Corresponding author address:* Dr. Warren E. Heilman, USDA Forest Service, Northern Research Station, 1407 S. Harrison Road, East Lansing, MI 48823.
E-mail: wheilman@fs.fed.us

wildfire in Colorado. The simulations revealed the sensitivity of fire spread rates to solar- and terrain-induced turbulent flow (e.g., daytime upslope flow).

Using both direct and large-eddy simulation (LES) techniques within the Weather Research and Forecasting Model (WRF), Cunningham et al. (2005) examined the structure and dynamics of buoyant plumes arising from surface heating sources similar to those that might be found during wildland fire episodes under a vertically sheared ambient atmospheric flow, a condition conducive to the mechanical generation of turbulence. The results from their simulations indicated that coherent vortical structures may develop in the vicinity of the heating sources, and that these vortices, which control the turbulent mixing within buoyant plumes, can also potentially lead to erratic fire behavior. Cunningham (2007) also used an LES version of WRF to simulate the effects of turbulent environments associated with density currents (e.g., thunderstorm outflows, sea-breeze fronts, cold fronts) on wildland fire plume behavior. The WRF simulations suggested that when ambient atmospheric winds oppose the motion of density currents (again a condition very conducive to turbulence generation), the vertical velocity within any buoyant plumes that are present can increase significantly and may, in turn, affect fire behavior.

Linn et al. (2007) used the Los Alamos National Laboratory High-Resolution Model for Strong Gradient Applications (HIGRAD) coupled with the "FIRETEC" fire behavior model to examine the effects of topography and topographically induced turbulent flow on wildland fire behavior. Their numerical simulations suggested that the rate of spread of wildland fires in complex terrain may be strongly influenced by interactions between the topography and the ambient wind field, which are known to contribute to enhanced, near-surface, ambient turbulence.

Sun et al. (2009) carried out a systematic study of the effects and importance of fire-induced circulations and ambient turbulence in the atmospheric boundary layer on the rate of spread of grassland fires using the University of Utah's Large-Scale Eddy Simulation (UU-LES) model (Zulauf 2001). They found that even though fire-induced turbulent convection was likely a more significant contributor to variability in the rates of spread of the grassland fires than ambient boundary layer turbulence, strong eddy circulations in the boundary layer can interact with fire-induced circulations to produce strong downdrafts behind fire lines, which are conducive to fire spread if they are able to persist. Bhutia et al. (2010) used atmospheric flow fields from the Sun et al. (2009) simulations to drive a firebrand combustion and trajectory model to demonstrate the effects of ambient atmospheric boundary layer and fire-induced turbulent circulations on firebrand transport and deposition, factors which contribute to erratic fire behavior.

In the area of in situ and remote sensing monitoring of wildland fire environments, including atmospheric turbulence effects, the recent experimental studies of Morandini et al. (2006), Clements et al. (2007, 2008), and Clements (2010) provide observational evidence of ambient atmospheric turbulence interactions with wildland fires and their induced turbulent circulations. Morandini et al. (2006) conducted a fire spread experiment in a plot of dense Mediterranean shrub vegetation with ambient near-surface wind speeds on the order of 4 m s$^{-1}$ and found that large-scale turbulence (length scales on the order of a few hundred meters) had a significant impact on flame shape, fire-environment temperatures, and the fire rate of spread. Near-surface atmospheric observations during and within a grass headfire experiment ($\sim$3 m s$^{-1}$ near-surface wind speeds) conducted by Clements et al. (2007, 2008) and Clements (2010) showed that fire-induced flows are highly complex and can interact with ambient turbulent flows in the boundary layer to produce regions of significant upward and downward vertical motions in the vicinity of fire lines.

Fire-induced turbulent circulations and their interactions with ambient turbulent circulations in the boundary layer have also been observed during more intense bushfires and crown fires. Sharples et al. (2012) noted that turbulent circulations over complex terrain and their interactions with fire-induced circulations may have been partly responsible for the observed fire channeling and spotting via ember transport during the January 2003 Alpine fires in southeastern Australia. During the intense crown fires of the "FROSTFIRE" experiment (Hinzman et al. 2003), Coen et al. (2004) concluded that rapid fire spread observed during the experiment was due to fire-induced turbulent circulations and not external ambient circulations. However, they noted some uncertainty in the atmospheric processes that were involved in the development of compensating downdrafts that supplied air for fire-induced convective updrafts via mass conservation. As noted by Sun et al. (2009), interactions between eddy circulations in the boundary layer and fire-induced plume circulations may play a role in the development of these compensating downdrafts.

These and other model- and observation-based studies have provided the scientific foundation and impetus for developing new turbulence-based fire-weather indices for tactical fire management that, with proper testing, could possibly be used alone or with other indices for indicating when and where atmospheric conditions may be conducive to erratic fire behavior.

Heilman and Bian (2010) carried out an initial study that examined the feasibility of using atmospheric mesoscale model predictions of near-surface turbulent kinetic energy per unit mass ($TKE_s$) (equal to one-half of the sum of the horizontal and vertical velocity variances; Stull 1988) in combination with the well-known Haines index (HI; Haines 1988) as the basis for a new fire-weather index ($HITKE_s = HI \times TKE_s$) that quantifies how conducive the atmosphere is to erratic fire behavior in the north-central and northeastern United States. Note that $TKE_s$ values are continuous while the HI takes on integer values ranging from 2 to 6, with higher integer values indicating dry and unstable air aloft. A full description of the HI and its surface-elevation-dependent calculation can be found in Haines (1988). The results from their study suggested that periods of rapid wildfire growth in this region are often associated with episodes of $TKE_s$ exceeding 3 $m^2 s^{-2}$ at the same time the HI is equal to 5 or 6 ($HITKE_s \geq 15 \ m^2 \ s^{-2}$). These conditions are indicative of a turbulent boundary layer sitting beneath unstable and dry atmospheric layers aloft. We are assessing the feasibility of using $TKE_s$ and $HITKE_s$ predictions for fire-weather applications in the western United States in a separate study. Feasibility tests in fire-prone areas outside the conterminous United States are still needed for potential applications of these indices there.

While Heilman and Bian (2010) provided a first step in 1) determining the association of significant atmospheric boundary layer turbulence with large fires and/or extreme and erratic fire behavior in one particular region of the United States and 2) determining the feasibility of using TKE alone or in combination with other indices like the HI as an indicator of how conducive the atmosphere may be to erratic fire spread in the United States, additional analyses are needed to determine when, where, and how often high turbulence episodes occur. Long-term climatological analyses of the HI based on gridded meteorological fields over North America have already been developed by Winkler et al. (2007) and Lu et al. (2011) and provide critical baseline information on the spatial and temporal patterns of the HI over the United States. A similar analysis is needed for $TKE_s$, especially if $TKE_s$ is used in combination with the HI and ultimately applied regionally or nationally as an additional fire-weather predictive tool. Determining the climatic variability of $TKE_s$ will provide critical baseline climatologies for comparisons with predicted and observed ambient TKE during actual wildfire events in the United States. It is through these comparisons that the effectiveness of TKE as a potential component of operational fire-weather indices and fire-weather forecasts can be assessed.

This study serves as a follow-up study to Heilman and Bian (2010), Winkler et al. (2007), and Lu et al. (2011) and provides an initial climatic assessment of the spatial variability of and temporal trends in $TKE_s$ across the United States based on 30 years of 3-hourly TKE data obtained from the North American Regional Reanalysis (NARR) dataset (Mesinger et al. 2006). Section 2 describes the NARR-based TKE climate analysis methodology used in this study. In section 3, we present computed average daily maximum $TKE_s$ and $HITKE_s$ values for each month, computed frequencies of occurrence of high $TKE_s$ and $HITKE_s$ for each month, the results of a near-surface flux Richardson number analysis to assess buoyancy and wind shear contributions to high $TKE_s$ episodes in the United States, and the temporal variability and long-term trends of $TKE_s$ and $HITKE_s$ in the United States. We conclude the paper in section 4 with a summary of the results and what they imply for potential turbulence-based fire-weather index applications in the United States.

## 2. Methods

The climatological analyses carried out in this study utilized data obtained from the National Centers for Environmental Prediction (NCEP) NARR dataset (Mesinger et al. 2006), a gridded and dynamically consistent atmospheric and land surface hydrology dataset that covers the 1979–present period. The NARR dataset integrates output data from the NCEP regional Eta Model (Janjić 1994) and its data assimilation system. Data are available every 3 h (0000, 0300, 0600, . . . , 2100 UTC) on a domain with 32-km horizontal grid spacing covering North America at 45 vertical levels. Input data for generating the NARR dataset include observations used in the NCEP–U.S. Department of Energy Global Reanalysis-2 Project (Kanamitsu et al. 2002), radar wind profiler data, Television and Infrared Observation Satellite (TIROS) Operational Vertical Sounder (TOVS)-1B radiances, additional precipitation data, and land surface and moisture data.

The TKE data incorporated into the NARR dataset are based on Eta Model predictions of TKE using the Mellor–Yamada level-2 and level-2.5 turbulence closure schemes (Mellor and Yamada 1974, 1982; Janjić 1994). The level-2 diagnostic scheme, applied to the surface layer in Eta Model simulations, assumes a balance between the production–consumption of TKE due to mechanical shear and buoyancy effects and the dissipation of TKE. The level-2.5 scheme, applied to atmospheric layers above the surface layer in Eta Model simulations, incorporates a prognostic equation for TKE

that accounts for advection, shear production, buoyancy production or consumption, diffusion, and dissipation of TKE.

For this study, TKE data at the NARR hybrid grid level 1 (12.0–21.7 m AGL) were used to quantify near-surface turbulent energy (i.e., $TKE_s$). Thirty years of TKE data at the hybrid grid level 1 were extracted from the NARR dataset at each 3-hourly interval from 0000 UTC 1 January 1979 through 2100 UTC 31 December 2008. These data provided the basis for developing a climatology of $TKE_s$ and examining its temporal variability over a subregion of North America that includes the conterminous United States (25°–50°N, 65°–125°W). Temperature, dewpoint temperature, wind speed, and 3-h averaged surface sensible heat flux data for the same 30-yr period were also extracted from the NARR dataset to compute $HITKE_s$ values and flux Richardson numbers $Ri_f$. These additional data were analyzed to compare the spatial and temporal variability of $TKE_s$ over the United States with the corresponding variability of $HITKE_s$. The data were also used to determine the relative contributions of wind shear and buoyancy in the production of near-surface turbulence over different regions of the United States. Although the feasibility of combining the HI and $TKE_s$ via a simple product of the two variables and using $HITKE_s$ as a potential fire-weather index has only been examined over the north-central and northeastern United States (Heilman and Bian 2010), a climatological analysis of $HITKE_s$ over the entire United States is also included in this study to provide baseline climatic information for ongoing and future assessments of $HITKE_s$ as a potential fire-weather index for application in other regions of the United States.

## 3. Results and discussion

### a. Average daily maximum $TKE_s$ and $HITKE_s$

Figure 1 shows the 30-yr (1979–2008) average daily maximum $TKE_s$ values for each month based on the 1979–2008 3-hourly NARR data. Near-surface TKE values typically reach a maximum during the daylight hours when wind shears and buoyancy usually reach their maximum values, although maximum $TKE_s$ values at night associated with strong nocturnal winds can also occur. The effects of terrain elevation on near-surface turbulence is clearly evident, with the highest average maximum $TKE_s$ values generally occurring over the Rocky Mountain and Appalachian Mountain regions of the United States for every month. Average daily maximum $TKE_s$ values exceeding 5 m² s⁻² are common over many locations in the Rocky Mountain region, with

the most extensive coverage of high $TKE_s$ values in this region occurring during the April–June period. Over isolated areas in the Appalachian Mountain region, average daily maximum $TKE_s$ values also exceed 5 m² s⁻². However, it is during the November–April period when average daily maximum $TKE_s$ values in this region tend to be the largest. This period encompasses the spring and autumn wildfire seasons in the northeastern United States. Over the central United States from Texas northward to the Dakotas, average daily maximum $TKE_s$ values [~(2.5–3.5) m² s⁻²] peak during the March–June period. During the late spring to early autumn period (May–September), near-surface turbulence is generally low over the southeastern United States; average daily maximum $TKE_s$ values during these months are less than 1 m² s⁻² in some areas.

Combining $TKE_s$ with the well-known HI via a simple product of the two values ($HITKE_s$) produces a new and relatively simple fire-weather index that may identify periods when dry and unstable atmospheric layers aloft are present (HI ≥ 5; see Haines 1988) at the same time substantial boundary layer turbulence exists ($TKE_s$ ≥ 3 m² s⁻²; see Stull 1988). This atmospheric condition ($HITKE_s$ ≥ 15 m² s⁻²; see Heilman and Bian 2010) may be conducive to erratic fire behavior not only through the direct impact of highly variable wind speeds and directions on fire spread but also through the enhanced downward turbulent mixing of dry, unstable, and high momentum air from aloft through the boundary layer and down to the surface. Like the average daily maximum $TKE_s$ values shown in Fig. 1, the average daily maximum $HITKE_s$ values across the United States also exhibit regional differences (Fig. 2). High daily maximum $HITKE_s$ values initially appear over northern Mexico and the Southwest in March and then spread northward through the Rocky Mountain region from April to August. Maximum values routinely exceed 15 m² s⁻² over many areas in the Rocky Mountain region. Over the eastern half of the United States, average maximum $HITKE_s$ values are usually less than 10 m² s⁻² throughout the year, except for parts of the Appalachian and the northeastern U.S. regions where average maximum values reach 12–14 m² s⁻² from December through April. Higher HI values over the Rocky Mountain region compared to over the eastern half of the United States during the late spring to early autumn seasons (Lu et al. 2011) contribute to the observed $HITKE_s$ patterns. These results suggest that the use of the 15 m² s⁻² threshold value (Heilman and Bian 2010) as an indicator of the atmospheric potential for extreme or erratic fire behavior because of concurrent anomalous atmospheric turbulence conditions and high HI values is probably more applicable for the eastern
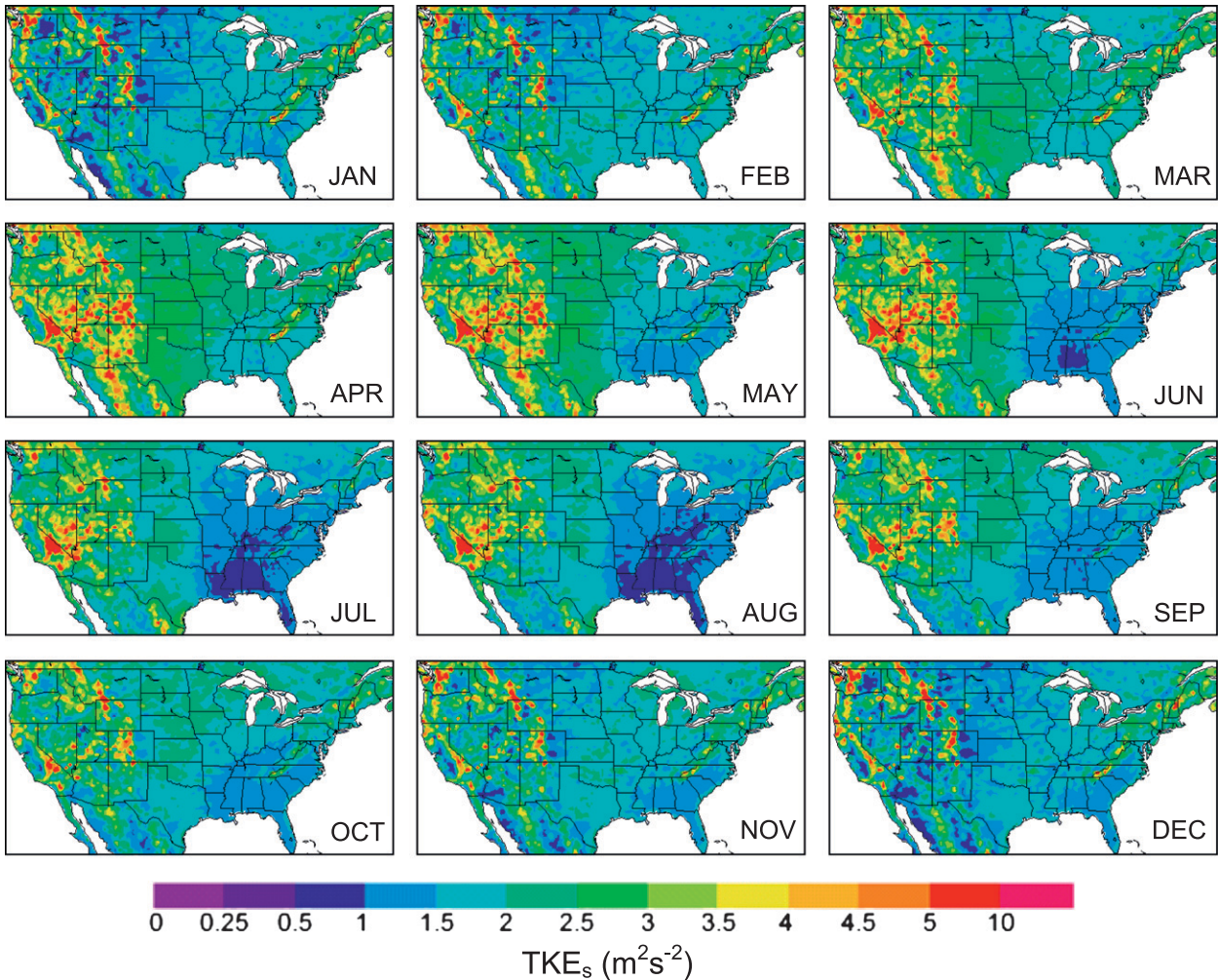
FIG. 1. Average daily maximum near-surface turbulent kinetic energy over the United States for each month based on 3-hourly NARR data for the 1979–2008 period.

half of the United States, and that a higher threshold on the order of 20–25 $m^2$ $s^{-2}$ may be needed for the western United States.

### b. Frequency of occurrence of high TKE$_s$ and HITKE$_s$

In addition to examining the spatial patterns in average daily maximum TKE$_s$ and HITKE$_s$ values across the United States, the frequencies of occurrence of high TKE$_s$ ($>3$ $m^2$ $s^{-2}$) and high HITKE$_s$ ($>15$ $m^2$ $s^{-2}$) values in the United States were also examined as part of the climatological analysis. A frequency of occurrence analysis provides insight into where, when, and how often high TKE$_s$ and HITKE$_s$ episodes occur in relation to known regional fire seasons and fire-prone locations.

The frequencies of occurrence of daily maximum TKE$_s$ values exceeding the 3 $m^2$ $s^{-2}$ threshold and daily maximum HITKE$_s$ values exceeding the 15 $m^2$ $s^{-2}$ threshold vary substantially from east to west across the United States. For daily maximum TKE$_s$ exceeding 3 $m^2$ $s^{-2}$ (Fig. 3), the highest frequencies of occurrence are found over the western United States; many locations there typically have more than 60% of the days in any given month with maximum TKE$_s$ exceeding the 3 $m^2$ $s^{-2}$ threshold. For most of the eastern United States, occurrences of daily maximum TKE$_s$ values greater than 3 $m^2$ $s^{-2}$ are fairly rare ($<10\%$ of the days each month). The exception is over the Appalachian Mountain and northeastern U.S. regions, where frequencies range from 30% to 60% during the November–May period. Over the Great Plains where grass fires are common, occurrences of maximum TKE$_s$ values exceeding 3 $m^2$ $s^{-2}$ are most likely during the March–June period (30%–50% of the days during those months).
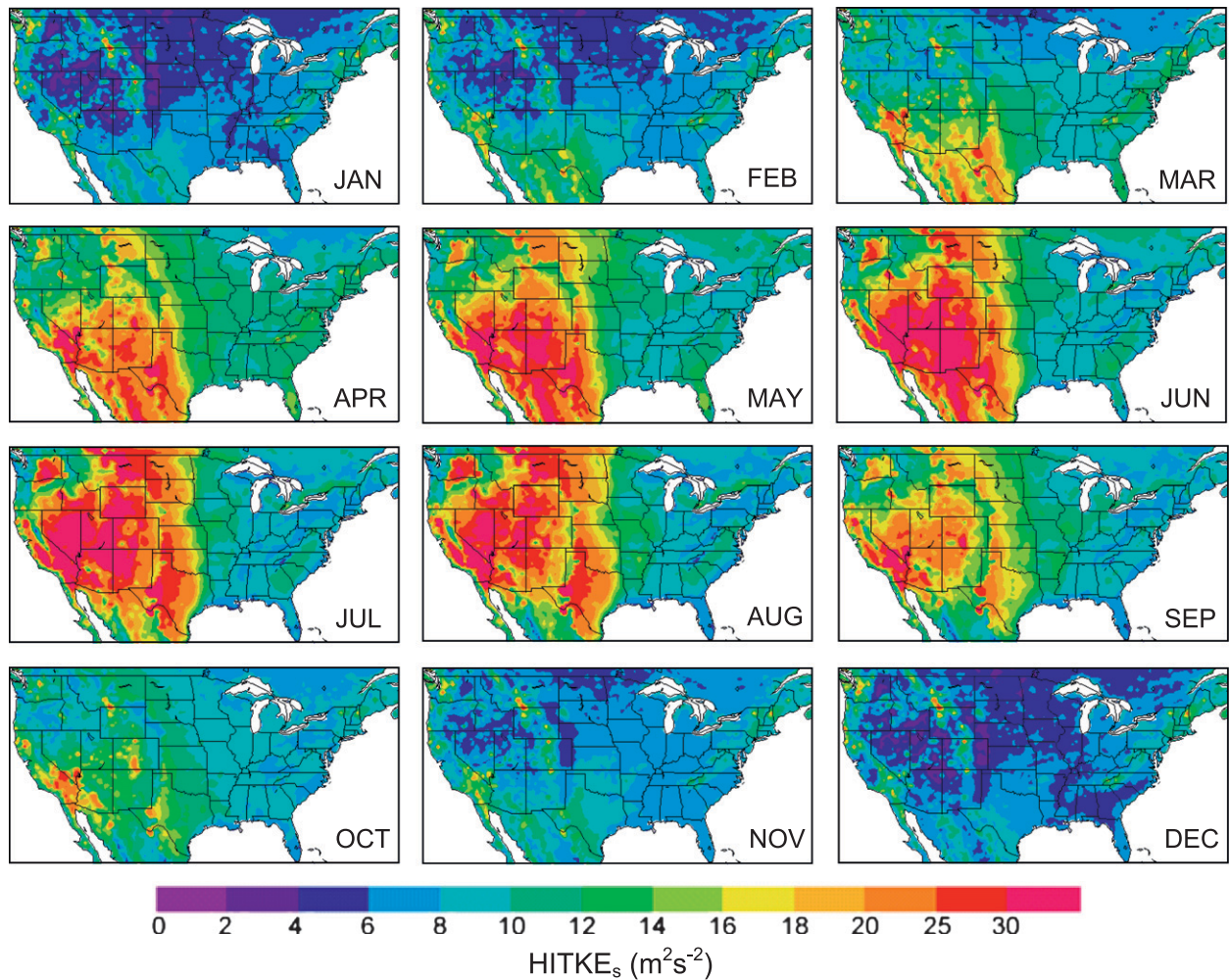
FIG. 2. Average daily maximum values of the product of the Haines index and near-surface turbulent kinetic energy (HITKE$_s$) over the United States for each month based on 3-hourly NARR data for the 1979–2008 period.

The frequency of occurrence of daily maximum HITKE$_s$ values exceeding 15 m$^2$ s$^{-2}$ (Fig. 4) has a similar spatial pattern to the high TKE$_s$ frequency pattern across the United States. The highest frequencies of occurrence are found over the western half of the United States, with frequencies in the 15%–30% range (i.e., 15%–30% of the days in a month have maximum HITKE$_s$ values that exceed the 15 m$^2$ s$^{-2}$ threshold). Figure 4 suggests that just east of the Rocky Mountains, in a band from southern Montana southward to eastern New Mexico, the frequency of occurrence of high HITKE$_s$ values is relatively low throughout the year. This is due primarily to the application of the high-elevation variant of the HI in this band and the application of the midelevation variant of the HI immediately to the east of this band, following the recommendation of Haines (1988). As shown in Lu et al. (2011), this results in average HI values within this general band that are

notably lower than the values over the Rocky Mountain range to the west and lower than the values over the western Great Plains. The eastern half of the United States, with the exception of the Appalachian Mountain region, typically has frequencies of occurrence of 2% or less. These frequencies are lower than the typical frequencies of occurrence of HI ≥ 5 over the western (40%–90%) and eastern (10%–40%) regions of the United States as reported by Winkler et al. (2007) and Lu et al. (2011) during the May–October time period. Over the Appalachian Mountains, high HITKE$_s$ values typically occur from November through April, with ~(10%–25%) of the days in those months having HITKE$_s$ values that exceed 15 m$^2$ s$^{-2}$.

c. *Buoyancy and wind shear contributions*

To assess the relative significance of wind shears and buoyancy in generating high TKE$_s$ values in the United
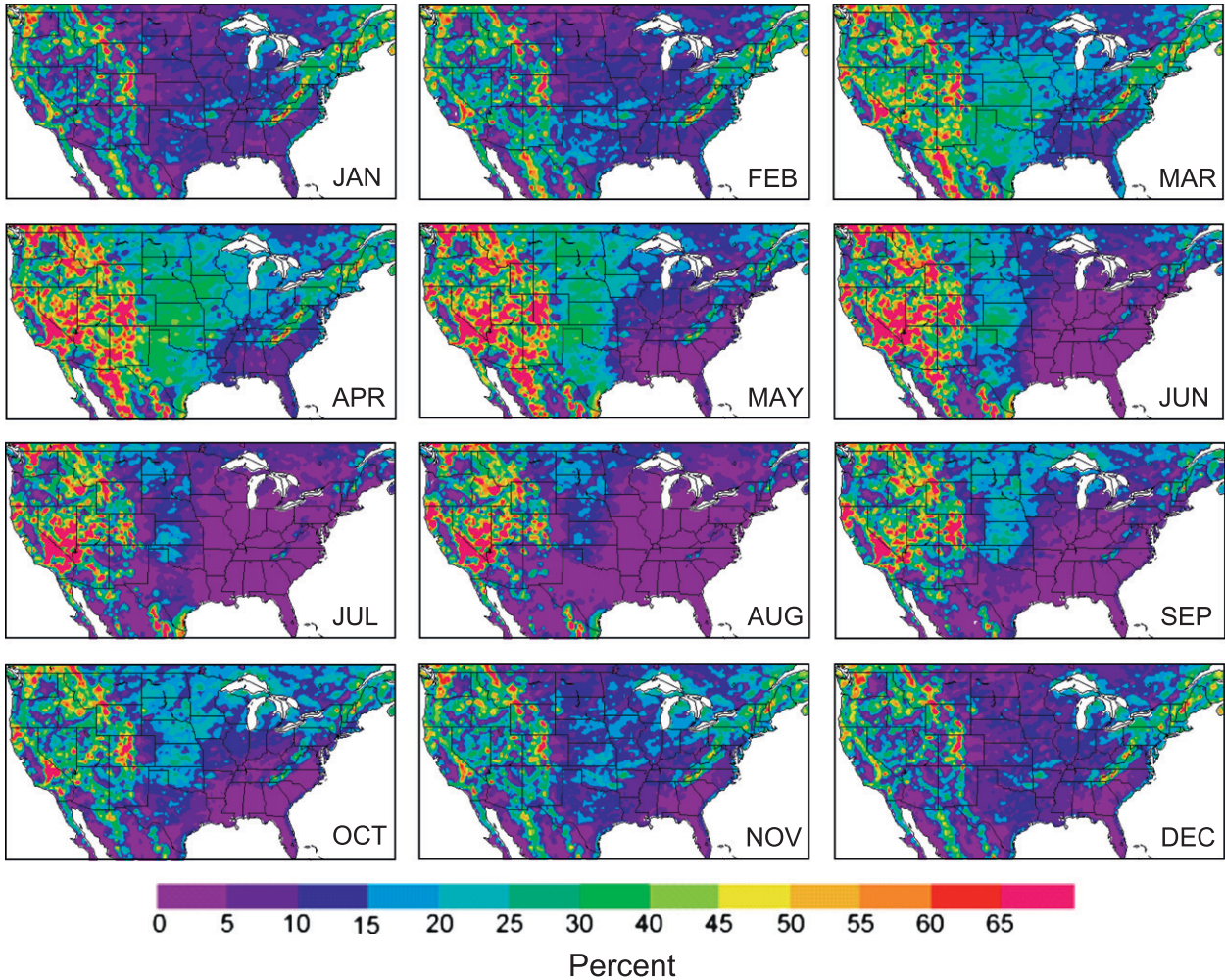
FIG. 3. Average percentage of days each month that have daily maximum TKE$_s$ > 3 m$^2$ s$^{-2}$ based on 3-hourly NARR data for the 1979–2008 period.

States, a hybrid near-surface Ri$_f$ analysis was carried out using the available NARR 3-h averaged surface sensible heat flux data and the instantaneous wind speed and temperature data valid every 3 h. Although using instantaneous sensible heat flux values along with instantaneous wind speed and temperature values to compute temporal Ri$_f$ patterns is preferable to using 3-h averaged flux data, the computations of Ri$_f$ values based on 3-h averaged sensible heat flux data in this study still provide insight into the overall significance of buoyancy compared to wind shears in generating the near-surface turbulence regimes suggested by the NARR TKE$_s$ data.

Figure 5 shows the average frequencies of occurrence of Ri$_f$ < −0.03 across the United States when daily maximum TKE$_s$ values exceed 3 m$^2$ s$^{-2}$ for each month using the 3-hourly NARR data. Flux Richardson numbers less than −0.03 are indicative of a buoyancy-dominated turbulence regime (Seinfeld 1975). During the months of December and January, buoyancy tends to be the dominant factor in generating high near-surface turbulence over the far southwestern and southeastern sections of the United States. The mechanical production of turbulence through wind shears under stable conditions (0.25 > Ri$_f$ > 0) tends to dominate near-surface turbulence regimes over most of the United States during December and January. Beginning in February, the spatial extent of buoyancy-dominated near-surface turbulence regimes starts to expand northward. By April, more than 60% of the high near-surface turbulence events over much of the western half of the United States tend to be dominated by the buoyant production of TKE. The buoyant production of near-surface turbulence is also dominant over the Appalachian Mountain region in the eastern United States by April. From May through August, buoyancy is the primary factor in generating high TKE$_s$ over most of the
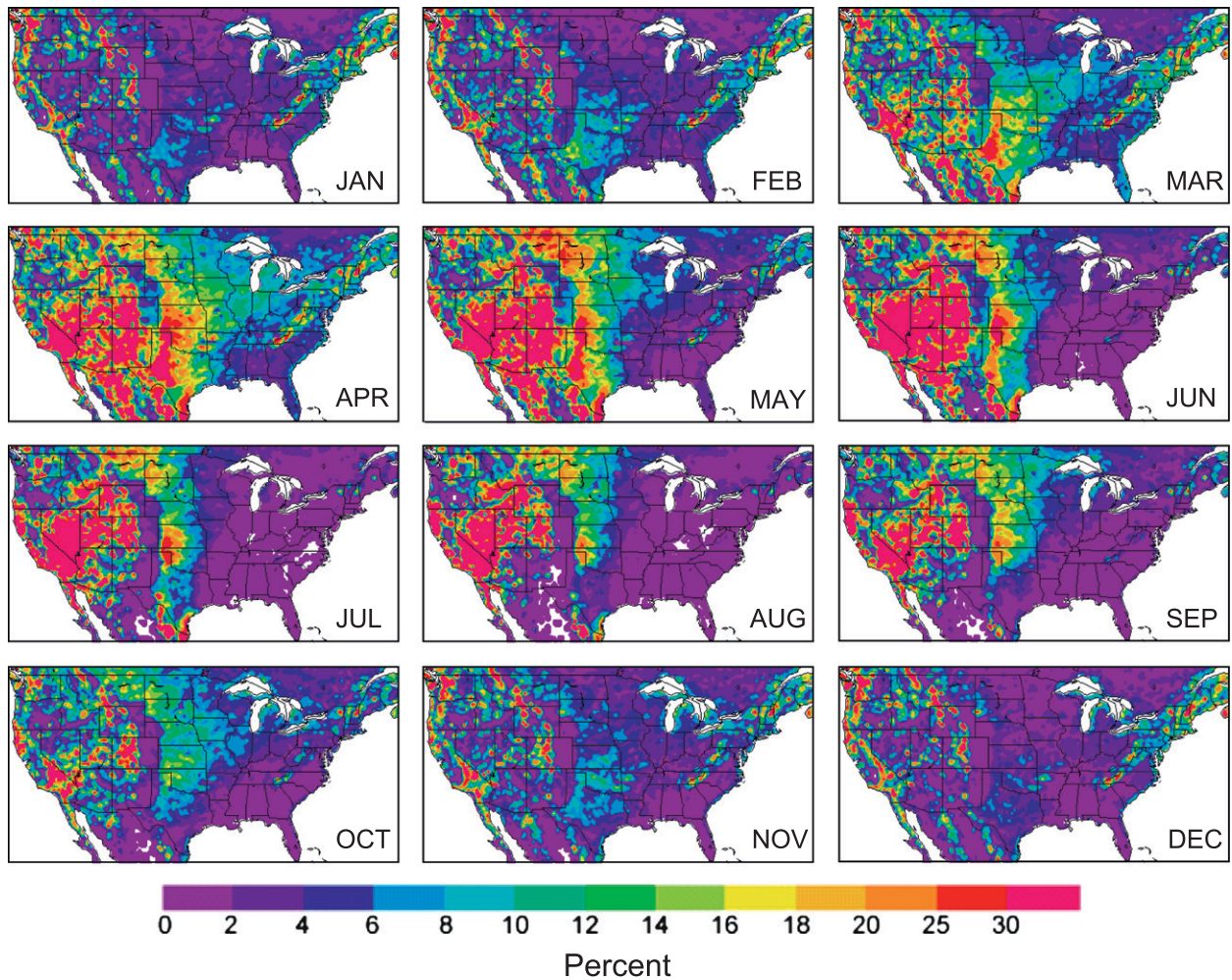
FIG. 4. As in Fig. 3, but for HITKE$_s$ > 15 m$^2$ s$^{-2}$.

United States except for isolated areas in the Midwest and Southeast, where near-surface wind shears play a substantial role. In particular, high near-surface turbulence events occurring over large portions of Mississippi and Alabama during the months of July and August tend to be associated with significant near-surface wind shears under stable conditions in the lower boundary layer just above the surface. Over the 1979–2008 period, on average less than 5% of the high near-surface turbulence events during July and August in these areas were associated with buoyancy-dominated turbulence regimes. From September through November, the spatial extent of buoyancy-dominated near-surface turbulence regimes over the United States diminishes, with only the southwestern and far southeastern regions of the United States exhibiting primarily buoyancy-dominated high near-surface turbulence events in November.

The Ri$_f$ frequency-of-occurrence maps shown in Fig. 5 suggest that even though wind shear is an important

factor in generating turbulence over high-terrain regions where near-surface wind speeds can be substantial, buoyancy is still the primary factor in generating high near-surface turbulence events over the western half of the United States during the May–October period. It is during this period that more than 90% of the wildfires in the western United States (31°–49°N, 101°–125°W) occur (Westerling et al. 2003). The maps also suggest that both buoyancy and wind shears play a significant role in generating high near-surface turbulence events during the spring and autumn months over many areas in the Midwest, Northeast, and Southeast. It is during these months when wildfires are most frequent in the eastern United States (Haines et al. 1975; Goodrick and Hanley 2009; Grala and Cook 2010).

### d. Temporal variability of TKE$_s$ and HITKE$_s$

To identify possible differences in the prominent periods or frequencies of variability in the 3-hourly NARR
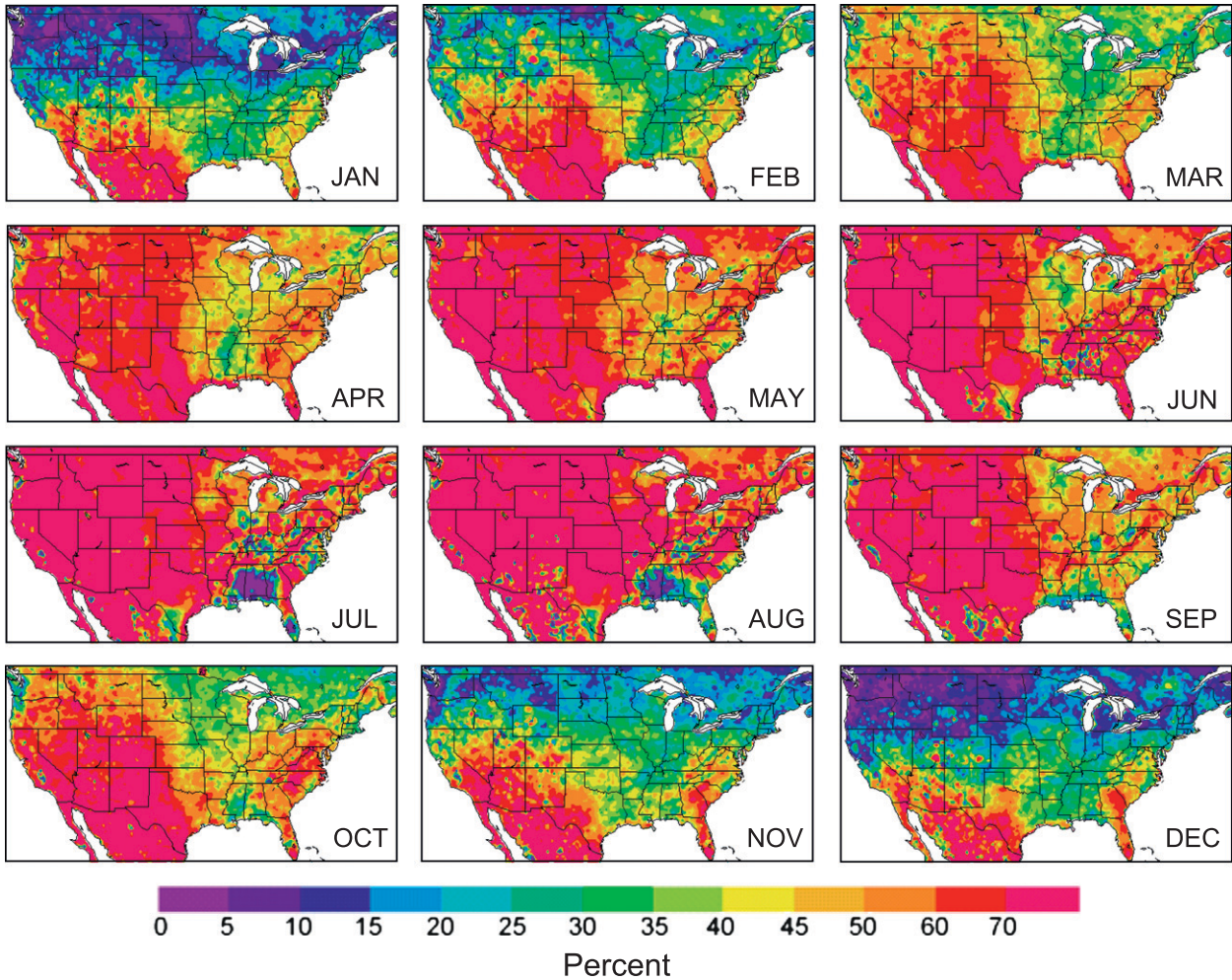
FIG. 5. Average frequency of occurrence of surface flux Richardson numbers $< -0.03$ with daily maximum $\mathrm{TKE}_s > 3$ $\mathrm{m^2\ s^{-2}}$ for each month based on 3-hourly NARR data for the 1979–2008 period.

$\mathrm{TKE}_s$ and computed $\mathrm{HITKE}_s$ time series that may exist in different regions of the United States, Fourier spectral analyses using a Hann tapering window were performed on the time series of regionally averaged $\mathrm{TKE}_s$ and $\mathrm{HITKE}_s$ values for arbitrarily defined northwest (37.5°–50°N, 95°–125°W), southwest (25°–37.5°N, 95°–125°W), northeast (37.5°–50°N, 65°–95°W), and southeast (25°–37.5°N, 65°–95°W) domains covering the conterminous United States. Although more sophisticated delineations of regional boundaries for this type of analysis are certainly possible, including climate-, topographic-, ecologic-, and fire-regime-based definitions, a simple broad-region definition approach was used in this initial climatic assessment.

The 30-yr time series of the 3-hourly regionally averaged $\mathrm{TKE}_s$ values for each defined region and the results of the Fourier spectral analyses of the time series are shown in Fig. 6. An annual cycle is evident in the plotted time series of regionally averaged $\mathrm{TKE}_s$ values (Figs. 6a,c,e,g) for all regions, and this annual cycle appears as a prominent peak in the Fourier spectral analyses (Figs. 6b,d,f,h) at a frequency of 1 $\mathrm{yr}^{-1}$ for all regions. Basic statistics for the individual time series (see Table 1) indicate that the northwest region had the highest overall mean $\mathrm{TKE}_s$ (1.049 $\mathrm{m^2\ s^{-2}}$) for the 30-yr period, and the southeast region had the lowest mean $\mathrm{TKE}_s$ (0.725 $\mathrm{m^2\ s^{-2}}$). The 30-yr mean $\mathrm{TKE}_s$ values for the northeast and southwest regions were similar (0.940 and 0.944 $\mathrm{m^2\ s^{-2}}$, respectively). The regional variations in mean $\mathrm{TKE}_s$ values differ from the regional variations in HI values (also shown in Table 1) in that the highest mean HI values occurred in the southwest (3.782) and southeast (3.595) regions.

A one-way analysis of variance (ANOVA) test and follow-up Tukey multiple comparison test on the observed mean values (normality test passed: $P > 0.05$;
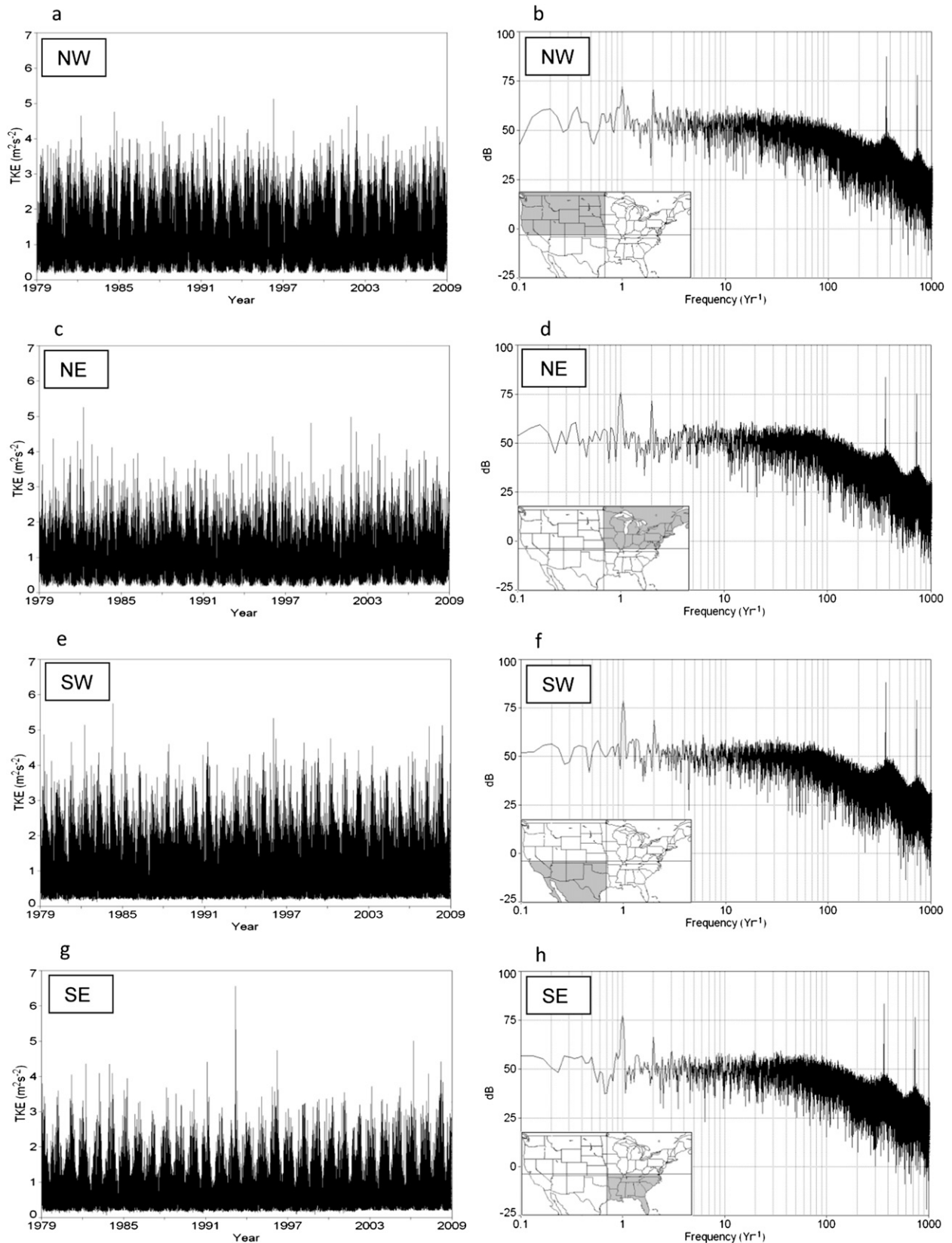
FIG. 6. (left) Time series and (right) Fourier frequency spectra of the domain averaged TKE$_s$ in the (a),(b) northwest, (c),(d) northeast, (e),(f) southwest, and (g),(h) southeast regions in the United States based on 3-hourly NARR data for the 1979–2008 period. The extent of each defined region (gray shading) is shown in the inset map within each frequency spectra figure.

TABLE 1. Basic statistics of the regionally averaged $TKE_s$, HI, and $HITKE_s$ for each region based on 3-hourly NARR data for the 1979–2008 period. Units for $TKE_s$ and $HITKE_s$ mean, maxima, minima, and standard deviations are meters squared per second squared. Hour values are in UTC and HI means and standard deviations are unitless.

| Index | Region | Mean | Std dev | Max | Hour and date of max | Min | Hour and date of min |
|---|---|---|---|---|---|---|---|
| $TKE_s$ | Northwest | 1.049 | 0.678 | 5.130 | 2100 24 Apr 1996 | 0.150 | 0600 29 May 1995 |
| | Northeast | 0.940 | 0.556 | 5.250 | 1800 3 Apr 1982 | 0.140 | 0600 9 Jul 1998 |
| | Southwest | 0.944 | 0.695 | 5.750 | 2100 25 Apr 1984 | 0.090 | 0900 15 Jan 1981 |
| | Southeast | 0.725 | 0.520 | 6.560 | 1800 13 Mar 1993 | 0.070 | 0300 1 Oct 1983 |
| HI | Northwest | 3.406 | 0.562 | 5.330 | 0000 17 Jul 2006 | 2.120 | 0000 30 Dec 2001 |
| | Northeast | 3.388 | 0.391 | 5.300 | 0000 2 May 1999 | 2.150 | 1200 28 Jan 1994 |
| | Southwest | 3.782 | 0.527 | 5.640 | 0000 20 May 2008 | 2.200 | 0600 4 Jan 1991 |
| | Southeast | 3.595 | 0.499 | 5.320 | 2100 22 Oct 1999 | 2.050 | 1200 20 Feb 2006 |
| $HITKE_s$ | Northwest | 3.388 | 2.421 | 18.460 | 2100 24 Apr 1996 | 0.470 | 0000 21 Dec 1995 |
| | Northeast | 3.072 | 1.901 | 17.670 | 1800 10 Mar 2002 | 0.460 | 0000 26 Sep 1982 |
| | Southwest | 3.516 | 2.817 | 24.480 | 2100 25 Apr 1984 | 0.280 | 0900 15 Jan 1981 |
| | Southeast | 2.532 | 1.910 | 23.310 | 1800 13 Mar 1993 | 0.280 | 0300 1 Oct 1983 |

equal variance test passed: $P = 0.884$) indicated a statistically significant ($P < 0.001$) difference in mean $TKE_s$ values among the different regions, with all regions differing from each other ($P < 0.001$) except for the northeast–southwest region comparison ($P = 0.985$). This is in contrast to the regional variations in mean HI values, where ANOVA and Tukey multiple comparison tests indicated all regions had statistically significant ($P < 0.001$) differences in mean HI values for the 1979–2008 period except for the northwest and northeast comparison ($P = 0.781$).

Annual peaks in the regionally averaged $TKE_s$ values were generally between 3 and 5 $m^2\,s^{-2}$, although a maximum regionally averaged value of 6.56 $m^2\,s^{-2}$ was observed in the southeast region at 1800 UTC 13 March 1993. The overall variability in the time series of regionally averaged $TKE_s$, as quantified by the standard deviation in $TKE_s$ values, is higher in the northwest (0.678 $m^2\,s^{-2}$) and southwest (0.695 $m^2\,s^{-2}$) regions than in the northeast (0.556 $m^2\,s^{-2}$) and southeast (0.520 $m^2\,s^{-2}$) regions.

The Fourier spectral analyses shown in Fig. 6 [expressed in terms of decibels (dB), where dB $= 10\,log_{10}(Re^2 + Im^2)$ and Re and Im are the real and imaginary components, respectively, of the fast Fourier transform at a given frequency] reveal statistically significant (99.9% critical limit) spectral peaks at frequencies (periods) of 1 $yr^{-1}$ (1 yr), 365 $yr^{-1}$ (24 h), and 730 $yr^{-1}$ (12 h) for all regions. In the northwest and southwest regions, the 1-$yr^{-1}$ frequency spectral component corresponds to maxima in the regionally averaged $TKE_s$ generally occurring during the months of April and May each year. However, in the northeast and southeast regions, the 1-$yr^{-1}$ spectral component corresponds to maxima in the regionally averaged $TKE_s$ occurring during the months of January and February each year. A 2-$yr^{-1}$

frequency (6-month period) spectral component in the $TKE_s$ time series is also evident in all regions, but its statistical significance varies from region to region (northwest: 50% critical limit; northeast: 95% critical limit; southwest: not statistically significant; southeast: not statistically significant). This 2-$yr^{-1}$ spectral component manifests itself in maxima in the regionally averaged $TKE_s$ for the northwest and northeast regions that tend to occur during the months of April and October each year. The general buoyancy production of $TKE_s$ during the daytime and the buoyancy consumption and dissipation of $TKE_s$ at night near the surface are responsible for the observed daily cycles (365-$yr^{-1}$ frequency spectral component) in $TKE_s$ across all regions. The times at which the maximum and minimum values of the regionally averaged $TKE_s$ values occurred in each region, as shown in Table 1, are consistent with the daytime and nighttime production–consumption and dissipation of $TKE_s$.

The corresponding temporal variability in the regionally averaged $HITKE_s$ values for each defined region is shown in Fig. 7. Averaging the 3-hourly $HITKE_s$ values displayed in each time series (Figs. 7a,c,e,g) over the 30-yr period indicates that the southwest region had the highest mean $HITKE_s$ value (3.516 $m^2\,s^{-2}$) followed by the northwest region (3.388 $m^2\,s^{-2}$), the northeast region (3.072 $m^2\,s^{-2}$), and finally the southeast region (2.532 $m^2\,s^{-2}$) (see Table 1). Because the regionally averaged 3-hourly $HITKE_s$ values for each region did not satisfy the normal distribution requirement for a one-way ANOVA test ($P = 0.008$), a Kruskal–Wallis one-way ANOVA on ranks test was carried out to determine the statistical significance of the difference in median $HITKE_s$ values among the regions (northwest: 3.402 $m^2\,s^{-2}$; northeast: 3.053 $m^2\,s^{-2}$; southwest: 3.503 $m^2\,s^{-2}$; southeast: 2.507 $m^2\,s^{-2}$). The differences
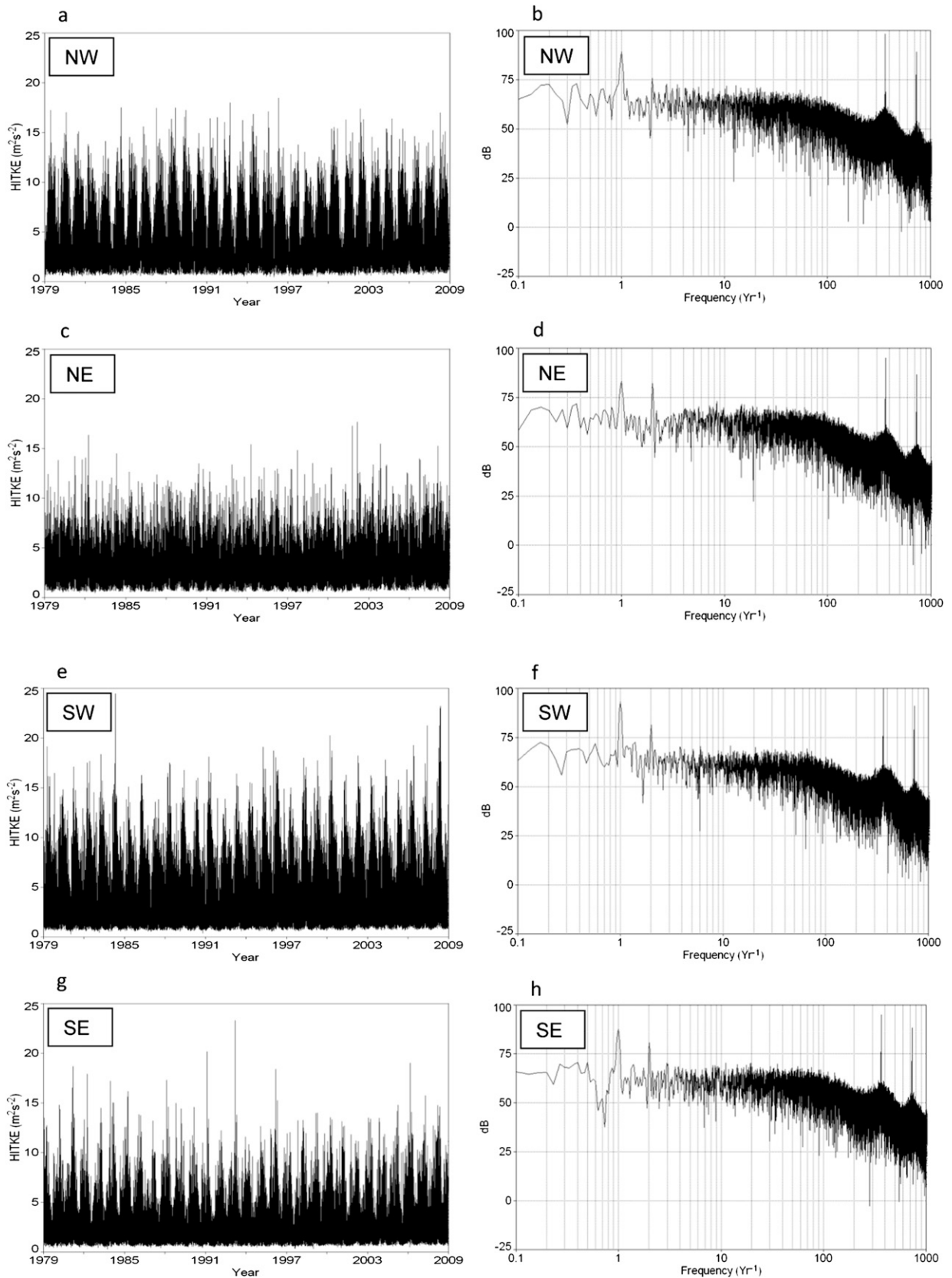
FIG. 7. As in Fig. 6, but for HITKE$_s$.

in median HITKE$_s$ values among the different regions were statistically significant ($P < 0.001$). A Tukey multiple comparison test on the ranks of the observed median HITKE$_s$ values indicated that all the regions differed from each other ($P < 0.05$) except for the northwest–southwest comparison ($P > 0.05$). This is in contrast to the comparisons of mean TKE$_s$ and HI values among the regions, which indicated the northeast and southwest regions did not have significantly different mean TKE$_s$ values while the northwest and northeast regions did not have significantly different mean HI values.

Annual peaks in the regionally averaged HITKE$_s$ values were generally between 12 and 20 m$^2$ s$^{-2}$. In the southwest region, there were seven occurrences during the 1979–2008 period when regionally averaged HITKE$_s$ values exceeded 20 m$^2$ s$^{-2}$. The southeast region had two such occurrences. Similar to the TKE$_s$ standard deviations, the standard deviations in the regionally averaged HITKE$_s$ values were higher in the northwest (2.421 m$^2$ s$^{-2}$) and southwest (2.817 m$^2$ s$^{-2}$) regions than in the northeast (1.901 m$^2$ s$^{-2}$) and southeast (1.910 m$^2$ s$^{-2}$) regions.

The Fourier spectral analyses of the HITKE$_s$ time series for each region (shown in Figs. 7b,d,f,h) indicate prominent and statistically significant annual (1-yr$^{-1}$ frequency), daily (365-yr$^{-1}$ frequency), and 12-h (730-yr$^{-1}$ frequency) cycles in every region, with each spectral peak exceeding the 99.9% critical limit. The 1-yr$^{-1}$ frequency spectral component corresponds to peaks in the regionally averaged HITKE$_s$ time series during the June–July period for the northwest region and during the month of May for the southwest region. These periods match the periods when regionally averaged HI values tend to reach their annual maxima in the northwest and southwest regions (time series not shown) but are slightly later than the April–May time period for the peaks associated with the 1-yr$^{-1}$ frequency spectral component in the time series of regionally averaged TKE$_s$ for the northwest and southwest regions. For both the northeast and southeast regions, the 1-yr$^{-1}$ frequency spectral component corresponds to peaks in the HITKE$_s$ time series primarily during the month of February, which generally coincides with the period when annual relative maxima in regionally averaged TKE$_s$ values associated with the TKE$_s$ 1-yr$^{-1}$ frequency spectral component occur. However, this is in contrast to peaks in regionally averaged HI values, which tend to occur during the June–July period in the northeast region and during the April–May and September–October period in the southeast region.

A statistically significant 2-yr$^{-1}$ (6 month) cycle in the time series of regionally averaged HITKE$_s$ is evident in the northeast (99% critical limit) and southeast (99.9%

critical limit) regions; the 2-yr$^{-1}$ cycle for HITKE$_s$ is not statistically significant in the northwest and southwest regions. Relative maxima in HITKE$_s$ values in the northeast and southeast regions associated with these 6-month cycles tend to occur during the months of April and October–November. It is the prominent 6-month cycle in the regionally averaged TKE$_s$ in the northeast region and the prominent 6-month cycle in the regionally averaged HI in the southeast region that generate the observed 6-month cycle for the regionally averaged HITKE$_s$ in both regions. The daily (365-yr$^{-1}$ frequency) and 12-h (730-yr$^{-1}$ frequency) cycles in the HI and TKE$_s$ time series contribute to the observed daily and 12-h cycles in the HITKE$_s$ time series.

Figure 8 shows the number of times over the 30-yr (1979–2008) period that the regionally averaged TKE$_s$ and HITKE$_s$ values reached their maximum for the year in a particular month for the northwest, northeast, southwest, and southeast regions. Evidence of the previously discussed general cyclic behavior of TKE$_s$ and HITKE$_s$ at the 6-month and yearly time scales can also be seen in these plots. The highest regionally averaged TKE$_s$ and HITKE$_s$ values in any year during the 1979–2008 period were more likely to occur during the month of April for the northwest, northeast, and southwest regions. In the southeast region, the highest values tended to occur during the February–April period. Occurrences of regionally averaged TKE$_s$ and HITKE$_s$ reaching their maximum values for the year in the summertime were rare in the northeast and southeast regions, whereas in the northwest and southwest regions, summertime occurrences were much more common. In particular, values of regionally averaged HITKE$_s$ in the northwest region reached their maximum during the June–September period for 16 out of the 30 years considered in this study.

*e. Long-term trends in TKE$_s$ and HITKE$_s$*

In addition to the Fourier spectral analyses carried out to identify prominent periods or frequencies of variability in the regionally averaged TKE$_s$ and HITKE$_s$ time series, 15-yr (1979–93, 1986–2000, 1994–2008) and overall 30-yr (1979–2008) trend (linear regression) analyses of TKE$_s$ and HITKE$_s$ were performed at each NARR grid point to determine whether there are locations or regions in the United States that experienced statistically significant positive or negative long-term trends in these indices. Statistical significance was determined using the $t$ statistic and the corresponding $P$ value calculated for $t$, which characterizes the probability of being wrong in concluding that there is a true association between the dependent variable (TKE$_s$ or HITKE$_s$ in this case) and the independent variable (year in this case). For $P < 0.05$, absolute values of the TKE$_s$
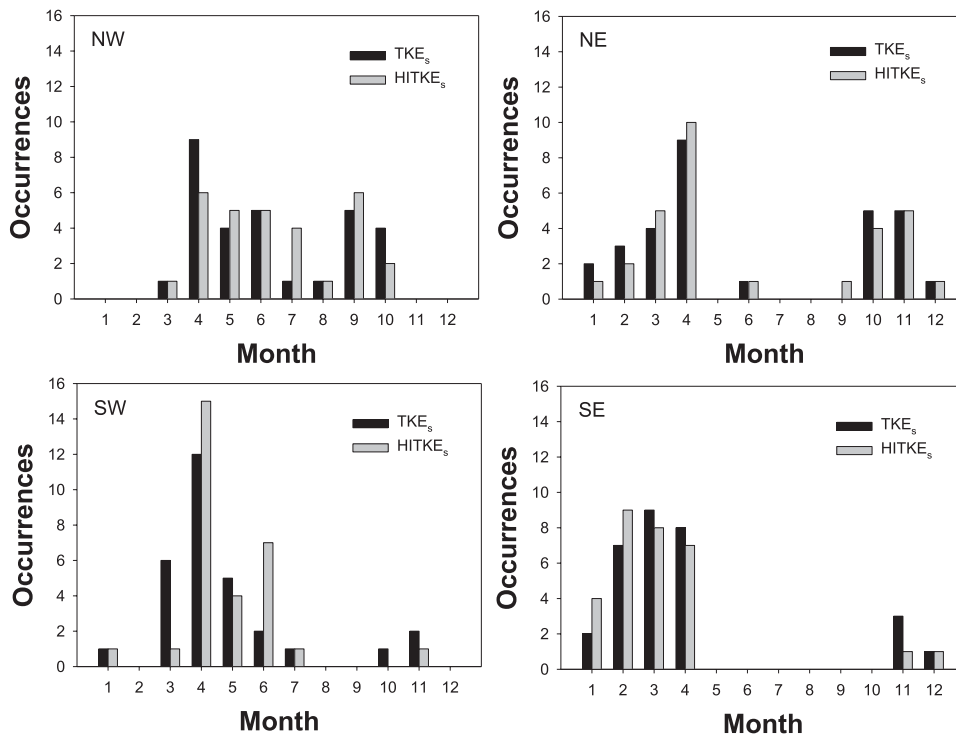
FIG. 8. Number of times over the 30-yr (1979–2008) period that regionally averaged $TKE_s$ and $HITKE_s$ values reached their maximum for the year in a particular month for the northwest, northeast, southwest, and southeast regions.

and $HITKE_s$ linear regression correlation coefficients $|R|$ had to be greater than 0.514 and 0.361 for the 15- and 30-yr trend analyses, respectively, for the linear regression slope values to be deemed statistically significant.

Figure 9 shows the values of the statistically significant slopes ($m^2 s^{-2} yr^{-1}$) of the linear regression lines fitted to the $TKE_s$ time series at each NARR grid point over the specified 15- and 30-yr time periods. Areas exhibiting statistically positive linear trends in $TKE_s$ were rather isolated during the 1979–93 period (Fig. 9a). However, broad areas over the southwestern and southeastern regions of the United States exhibited positive trends during the 1986–2000 period (Fig. 9b), and a large area extending from the southeastern United States through the central and northern Great Plains to the northwestern sections of the United States exhibited positive trends during the 1994–2008 period (Fig. 9c). The linear trends ranged from 0.007 to 0.020 $m^2 s^{-2} yr^{-1}$ (from 0.105 to 0.300 $m^2 s^{-2}$ over the 15-yr periods) in these areas. Very few areas exhibited statistically significant negative trends in $TKE_s$ over the specified periods. When considering the entire 1979–2008 period (Fig. 9d), most of the United States was characterized by statistically significant positive trends in $TKE_s$. Only the New England region, a narrow area from southern Texas northeastward to eastern Iowa, and the interior Rocky

Mountain region exhibited no trends or negative trends over the 30-yr period.

The spatial patterns of site-specific positive and negative trends in $TKE_s$ over the specified 15- and 30-yr periods shown in Fig. 9 can be summarized on a broader regional basis using the previously defined northwest, northeast, southwest, and southeast regions (see insets in Fig. 6). Figure 10 shows the regionally averaged annual-mean $TKE_s$ values and their corresponding 1979–93, 1986–2000, 1994–2008, and 1979–2008 linear trends for each region. Summary statistics for the $TKE_s$ trends are listed in Table 2. The 1979–2008 linear trends in $TKE_s$ were all positive and statistically significant ($P < 0.05$) in the northeast (0.0021 $m^2 s^{-2} yr^{-1}$), southwest (0.0021 $m^2 s^{-2} yr^{-1}$), and southeast (0.0030 $m^2 s^{-2} yr^{-1}$) regions (Figs. 10b–d). The 30-yr linear trend in the northwest region (0.0015 $m^2 s^{-2} yr^{-1}$) was also positive, but not statistically significant ($P = 0.097$) (Fig. 10a). In all regions except the southwest region, the largest positive 15-yr trends in $TKE_s$ values occurred during the 1994–2008 period. The overall 1994–2008 trends were highest in the eastern U.S. regions, with values of 0.0079 and 0.0076 $m^2 s^{-2} yr^{-1}$ characterizing the northeast and southeast regions, respectively.

Figures 11a–d show the corresponding 15- and 30-yr trends in $HITKE_s$ across the United States. The general
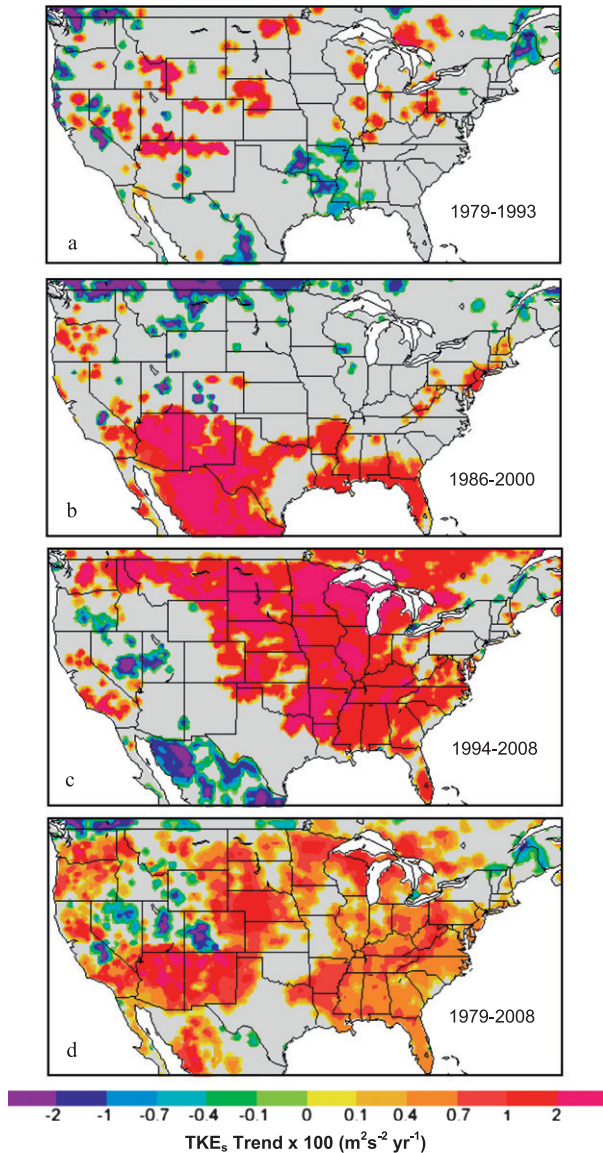
FIG. 9. Statistically significant linear trends in TKE$_s$ as quantified by slope values ($\Delta$TKE$_s$ yr$^{-1}$) of linear regression lines fitted to the TKE$_s$ times series at each NARR grid point over the (a) 1979–93, (b) 1986–2000, (c) 1994–2008, and (d) 1979–2008 periods. Slope values were multiplied by 100, and areas shaded in gray represent areas where slope values were not statistically significant.

spatial patterns of significant positive and negative linear trends in HITKE$_s$ are similar to the spatial patterns of TKE$_s$ trends, although the total area exhibiting significant positive linear trends in HITKE$_s$ values is diminished somewhat relative to that for TKE$_s$. This is due to rather limited and isolated areas across the United States that exhibited significant 15- and 30-yr positive linear trends in HI values (not shown). Those areas included central Nevada and northern New Mexico from

1979 to 1993; southern New Mexico, northwestern Texas, and southern Louisiana from 1986 to 2000; Northern California, western Nevada, and the northern Great Plains from 1994 to 2008; and western Nevada, Arizona, New Mexico, eastern Colorado, and Alabama over the entire 1979–2008 period. Broad areas in the Southeast, the western Great Lakes region, the northern Great Plains, and the Southwest exhibited positive linear trends in HITKE$_s$ values that exceeded 0.07 m$^2$ s$^{-2}$ yr$^{-1}$ during the 1986–2000 and 1994–2008 periods (Figs. 11b,c). When considering the entire 1979–2008 period, the statistically significant linear trend values ranged from 0.01 to 0.04 m$^2$ s$^{-2}$ yr$^{-1}$ (0.3–1.2 m$^2$ s$^{-2}$ increase over 30 years) over much of the eastern United States (Fig. 11d). Larger linear trends characterized some areas in the Southwest and central Great Plains, with values exceeding 0.1 m$^2$ s$^{-2}$ yr$^{-1}$ (3 m$^2$ s$^{-2}$ increase over 30 years) over parts of Arizona and New Mexico.

The broader regional-scale trends in HITKE$_s$ shown in Fig. 12 (summary statistics also listed in Table 2) reflect the same general trends as those for TKE$_s$ shown in Fig. 10. The largest positive 15-yr HITKE$_s$ trends occurred during the 1994–2008 period for all regions except the southwest region, where the largest increase occurred during the 1986–2000 period. Like the TKE$_s$ trends, the overall 1994–2008 trends were highest in the eastern U.S. regions with values of 0.0289 and 0.0335 m$^2$ s$^{-2}$ yr$^{-1}$ in the northeast and southeast regions, respectively. The 30-yr trends were positive in all regions and statistically significant ($P < 0.05$) in every region except the northwest region ($P = 0.299$). However, in contrast to the largest regional-scale 30-yr TKE$_s$ trend that occurred in the southeast region, the largest regional-scale 30-yr HITKE$_s$ trend occurred in the southwest region (0.0120 m$^2$ s$^{-2}$ yr$^{-1}$).

## 4. Summary and conclusions

As a follow-up study to the work of Winkler et al. (2007), Heilman and Bian (2010), and Lu et al. (2011), we have examined the spatial and temporal variability of TKE$_s$ and HITKE$_s$ values across the United States using 1979–2008 data extracted from the NCEP–NARR dataset to provide a baseline climatology of these indices that can be used for comparison with predicted and observed TKE$_s$ and HITKE$_s$ values during actual wildfire and fire-weather episodes. It is through these comparisons that the effectiveness of TKE as a potential component of operational fire-weather indices can be assessed and appropriate thresholds set for TKE-based indices such that index values exceeding these thresholds actually signify anomalous and potentially dangerous fire-weather conditions.
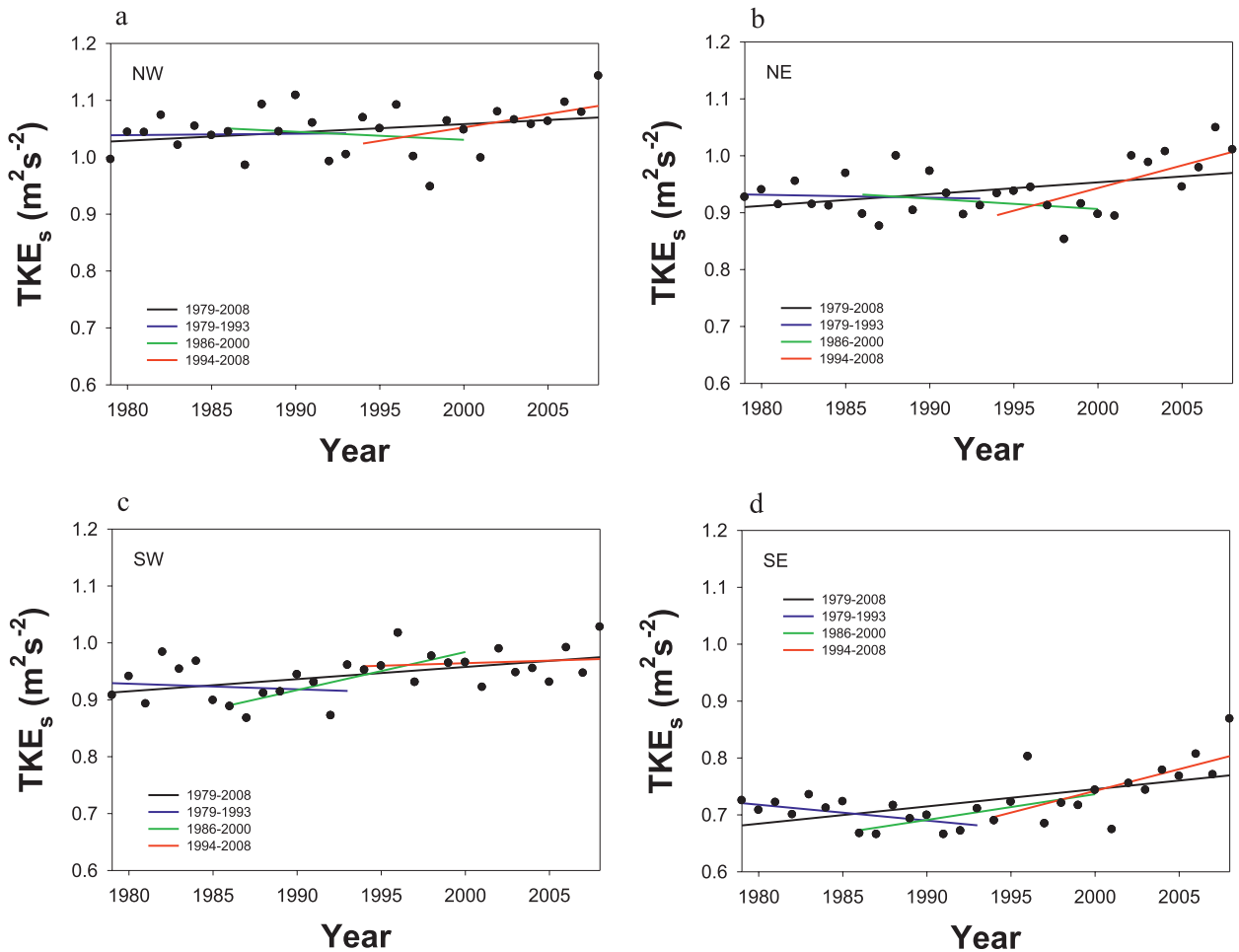
FIG. 10. Regionally averaged annual mean TKE$_s$ values (dots) and the 1979–2008, 1986–2000, 1994–2008, and 1979–2008 linear trends represented as linear regression lines for the (a) northwest, (b) northeast, (c) southwest, and (d) southeast regions. Slope values, linear regression correlation coefficients, and $P$ values for the linear regression lines are shown in Table 2.

The analyses of the spatial and temporal patterns of TKE$_s$ and HITKE$_s$ based on the 1979–2008 NARR data suggest that there are substantial regional differences in these indices across the United States. Average daily maximum TKE$_s$ values and occurrences of daily maximum TKE$_s$ values exceeding 3 m$^2$ s$^{-2}$, a threshold indicative of a highly turbulent lower-atmospheric boundary layer, are highest over the high-elevation Rocky Mountain and Appalachian Mountain regions. Over the Rocky Mountain region, even occurrences of daily maximum TKE$_s$ values exceeding 5 m$^2$ s$^{-2}$ are common throughout the year, although it is during the April–June period when the most extensive spatial coverage of high TKE$_s$ values occurs in this region. High TKE$_s$ values over the Appalachian Mountain region tend to occur during the November–April period. Daily maximum TKE$_s$ values in the southeastern United States during the summer months tend to be quite low (0.5–1.5 m$^2$ s$^{-2}$), largely the

result of reduced buoyancy production of near-surface turbulence in this area during the summer months (as suggested by the preponderance of observed positive Ri$_f$ values during high TKE$_s$ events).

Average daily maximum HITKE$_s$ values routinely exceed 15 m$^2$ s$^{-2}$ over many areas in the Rocky Mountain region during the April–September period, while values are usually less than 10 m$^2$ s$^{-2}$ over the eastern half of the United States throughout the year, except for parts of the Appalachian Mountain and northeastern U.S. regions. Typically, the 15 m$^2$ s$^{-2}$ threshold is exceeded on more than 60% of the days each month over much of the Rocky Mountain region during the April–September period. Exceedances of the 15 m$^2$ s$^{-2}$ threshold over much of the eastern United States are much less frequent (<10% of the days each month). The relatively high frequency of HITKE$_s$ values exceeding 15 m$^2$ s$^{-2}$ over the Rocky Mountain region makes the

TABLE 2. Slopes ($m^2 \, s^{-2} \, yr^{-1}$), linear regression correlation coefficients $R$ and probability $P$ values for the regionally averaged annual mean $TKE_s$ and $HITKE_s$ linear regression lines shown in Figs. 10 and 12, respectively.

| Region | Period | Slope ($TKE_s$) | $R$ ($TKE_s$) | $P$ ($TKE_s$) | Slope ($HITKE_s$) | $R$ ($HITKE_s$) | $P$ ($HITKE_s$) |
|---|---|---|---|---|---|---|---|
| Northwest | 1979–93 | +0.0002 | +0.030 | 0.914 | +0.0041 | +0.119 | 0.674 |
| | 1986–2000 | −0.0014 | −0.140 | 0.618 | −0.0169 | −0.372 | 0.172 |
| | 1994–2008 | +0.0047 | +0.457 | 0.087 | +0.0195 | +0.475 | 0.074 |
| | 1979–2008 | +0.0015 | +0.309 | 0.097 | +0.0037 | +0.196 | 0.299 |
| Northeast | 1979–93 | −0.0005 | −0.069 | 0.808 | +0.0015 | −0.047 | 0.868 |
| | 1986–2000 | −0.0018 | −0.221 | 0.428 | −0.0083 | −0.255 | 0.359 |
| | 1994–2008 | +0.0079 | +0.665 | 0.007 | +0.0289 | +0.701 | 0.004 |
| | 1979–2008 | +0.0021 | +0.401 | 0.028 | +0.0082 | +0.430 | 0.018 |
| Southwest | 1979–93 | −0.0010 | −0.123 | 0.661 | −0.0052 | −0.175 | 0.532 |
| | 1986–2000 | +0.0067 | +0.728 | 0.003 | +0.0293 | +0.671 | 0.006 |
| | 1994–2008 | +0.0009 | +0.131 | 0.642 | +0.0070 | +0.183 | 0.513 |
| | 1979–2008 | +0.0021 | +0.479 | 0.007 | +0.0120 | +0.549 | 0.002 |
| Southeast | 1979–93 | −0.0029 | −0.529 | 0.043 | −0.0129 | −0.561 | 0.030 |
| | 1986–2000 | +0.0045 | +0.560 | 0.030 | +0.0176 | +0.518 | 0.048 |
| | 1994–2008 | +0.0076 | +0.654 | 0.008 | +0.0335 | +0.714 | 0.003 |
| | 1979–2008 | +0.0030 | +0.571 | <0.001 | +0.0116 | +0.548 | 0.002 |

use of the 15 $m^2 \, s^{-2}$ $HITKE_s$ threshold proposed by Heilman and Bian (2010) as a possible operational indicator of the atmospheric potential for extreme or erratic fire behavior in the north-central and northeastern United States somewhat problematic over the western United States. A higher $HITKE_s$ threshold on the order of 20–25 $m^2 \, s^{-2}$ may be more applicable for the western United States so that exceedances of the threshold truly represent anomalous near-surface atmospheric turbulence conditions concurrent with dry and unstable atmospheric layers aloft. The initial findings of Heilman and Bian (2008) in their comparisons of $TKE_s$ and $HITKE_s$ evolution with fire spread during the 1988 western U.S. Yellowstone fires suggest that, indeed, higher thresholds are probably needed; $TKE_s$ and $HITKE_s$ values sometimes exceeded 6 and 25 $m^2 \, s^{-2}$, respectively, during the most significant Yellowstone fire spread episodes.

More research, including comparisons of $TKE_s$ and $HITKE_s$ evolution with observed fire spread rates during wildland fire episodes in all regions of the United States, is needed to identify appropriate region- or state-specific threshold values that would be critical for ultimately adopting an index like $HITKE_s$ as an operational fire-weather index. Also, new research that utilizes coupled fire–atmosphere modeling systems applied to wildland fire events in all regions of the United States may provide opportunities for examining possible regional differences in how turbulence dynamics (including turbulence aloft) affect fire spread, identifying regional differences in the correlations of $HITKE_s$ variability with fire spread, and developing more sophisticated turbulence-based fire-weather indices that also take into account turbulent conditions throughout the boundary layer.

The climatological spatial and temporal patterns of $TKE_s$ and $HITKE_s$ over the United States show general agreement with the regionally dependent fire seasons that characterize the United States. Over the northwest and southwest regions of the United States, average daily maximum $TKE_s$ and $HITKE_s$ values and the frequencies of occurrence of high $TKE_s$ and $HITKE_s$ values are generally largest during the April–September period, which overlaps the western U.S. June–September fire season. Over the northeast and southeast regions, and particularly over the Appalachian Mountain areas, the corresponding values and frequencies are largest during the November–April period; the autumn and spring fire seasons for these regions overlap this period.

The NARR data suggest that buoyancy is the primary mechanism for turbulence generation during episodes of significant near-surface turbulence ($TKE_s$ values exceeding 3 $m^2 \, s^{-2}$ and $HITKE_s$ exceeding 15 $m^2 \, s^{-2}$) over the western half of the United States from May to October, which overlaps the western U.S. fire season. The NARR data also suggest that during the spring and autumn wildfire seasons in the eastern United States, both buoyancy and wind shears play a significant role in turbulence generation during high near-surface turbulence events. Because buoyancy is such an important factor in shaping near-surface turbulence regimes, relying only on observed or predicted mean wind fields and associated wind shears to quantify or characterize near-surface ambient turbulence energy for calculating turbulence-based fire-weather indices like $HITKE_s$ may be inadequate. With predictions of TKE that fully account for both wind shear and buoyancy effects on TKE production now readily available as part of the suite of
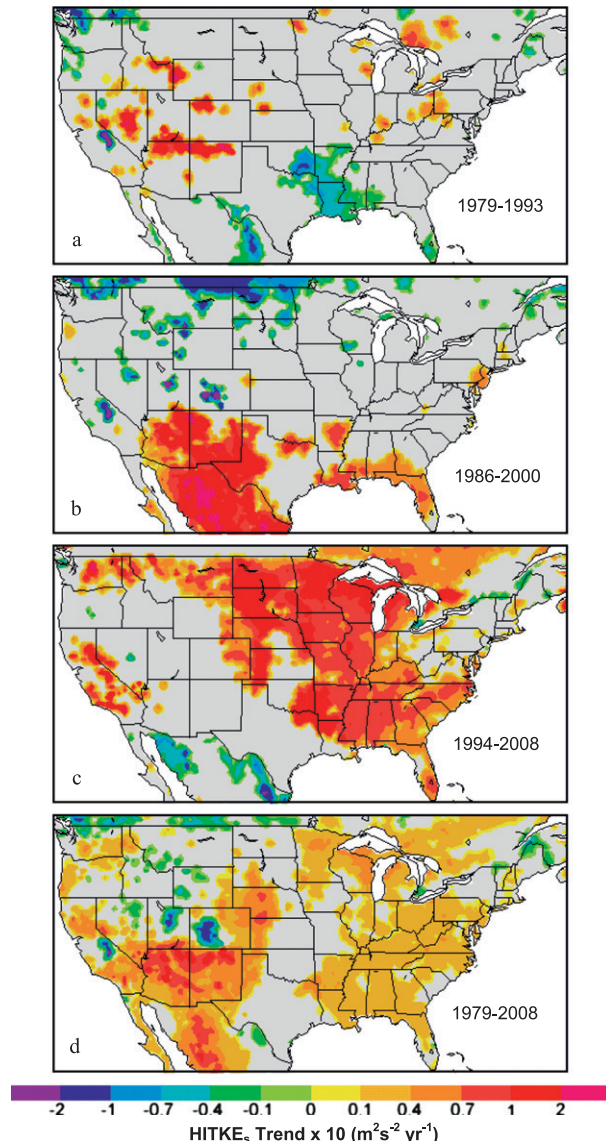
FIG. 11. As in Fig. 9, but for HITKE$_s$. Slope values were multiplied by 10.

output variables from current operational and research-based atmospheric models, providing predictions of turbulence-based indices like HITKE$_s$ for fire-weather applications is now feasible.

The temporal variability exhibited in the times series of regionally averaged 3-hourly NARR TKE$_s$ and HITKE$_s$ data over the 1979–2008 period indicates that there are important regional differences in the temporal behavior of these indices over the United States. In all regions, there are statistically significant annual, daily, and 12-hourly cycles that contribute to the overall observed temporal variability in TKE$_s$ and HITKE$_s$. Annual cycles in the TKE$_s$ time series in the north-western and southwestern regions of the United States

contribute to the general observed pattern of peak values during April and May, while annual cycles in the northeastern and southeastern regions contribute to peak values during January and February. Annual cycles in HITKE$_s$ are similar to the TKE$_s$ annual cycles in each region, except for the northwest region where peak HITKE$_s$ values tend to occur slightly later than peak TKE$_s$ values (June and July instead of April and May). There are also significant 6-month cycles that contribute to the TKE$_s$ temporal variability in the northeast region and to the HITKE$_s$ temporal variability in the northeast and southeast regions. The 6-month cycles are generally manifested in secondary peaks in TKE$_s$ values during April and October for the northeast region and secondary peaks in HITKE$_s$ values also during April and October for the northeast and southeast regions. The 6-month cycles and the timing of peak value occurrences in the TKE$_s$ and HITKE$_s$ time series for the northeast region coincide with the northeast spring and autumn wildfire seasons. Further research is needed to examine the temporal variability of TKE$_s$ and HITKE$_s$ over more refined regions, such as defined regions based on fire-regime considerations.

Finally, the observed 30-yr (1979–2008) linear trends in TKE$_s$ and HITKE$_s$ indicate that values of these indices have generally increased over large areas in the United States, including much of the mid-Atlantic, Southeast, Midwest, Great Plains, Southwest, and Pacific Northwest regions. General increases in these indices during the first 15 years (1979–93) of this 30-yr period were limited to rather small isolated areas throughout the United States. However, positive linear trends during the 1986–2000 and 1994–2008 periods were significant over large areas of the United States. The southern tier of states experienced statistically significant increases during the 1986–2000 period, while a broad area extending from the Southeast through the northern Great Plains and into the northern Rocky Mountain region experienced statistically significant increases during the 1994–2008 period.

Using a subset of the NARR data over the 1979–2006 period, Pryor et al. (2009) found generally positive trends in near-surface wind speeds at 0000 UTC at many locations in the United States, an indication of potential increases in wind shear. However, the areas exhibiting increasing trends in TKE$_s$ in this study were somewhat broader. This suggests that increasing trends in atmospheric instability (i.e., buoyancy) near the surface over large areas of the United States associated with anomalous warming may be the primary factor responsible for the observed increasing trends in NARR TKE$_s$ and HITKE$_s$ values over many areas of the United States. Further research is needed to actually ascertain the relative importance of buoyancy trends in comparison with
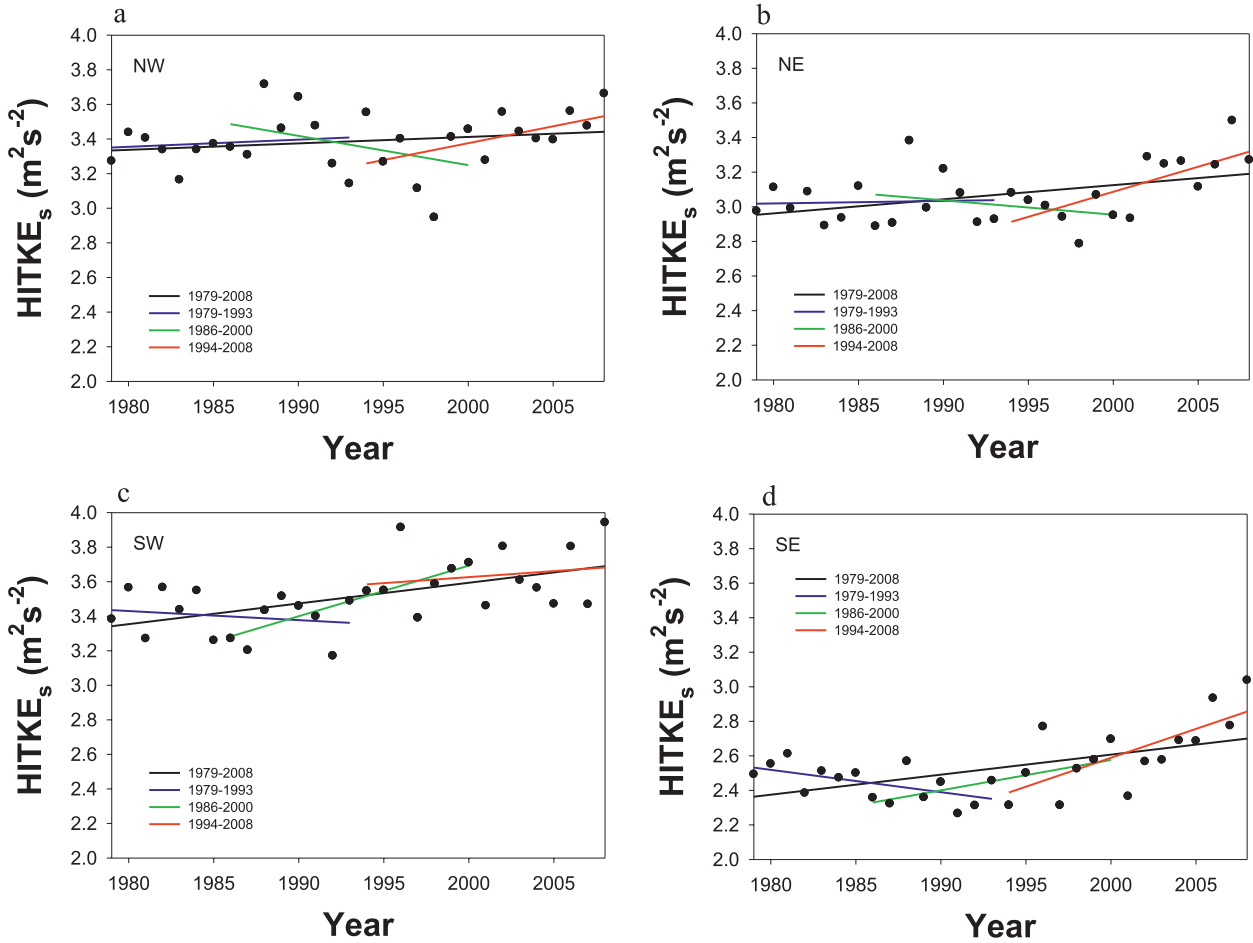
FIG. 12. As in Fig. 10, but for HITKE$_s$.

wind shear trends over the United States in contributing to the observed trend patterns in TKE$_s$ and HITKE$_s$.

REFERENCES

Andrews, P. L., 1986: BEHAVE: Fire behavior prediction and fuel modeling system-BURN subsystem Part 1. USDA Forest Service, Intermountain Research Station General Tech. Rep. INT-194, Ogden, UT, 130 pp. [Available online at http://www.fs.fed.us/rm/pubs_int/int_gtr194.pdf.]

Bhutia, S., M. A. Jenkins, and R. Sun, 2010: Comparison of firebrand propagation prediction by a plume model and a coupled–fire/atmosphere large–eddy simulator. *J. Adv. Model. Earth Syst.,* **2,** doi:10.3894/JAMES.2010.2.4.

Clark, T. L., J. Coen, and D. Latham, 2004: Description of a coupled atmosphere–fire model. *Int. J. Wildland Fire,* **13,** 49–63.

Clements, C. B., 2010: Thermodynamic structure of a grass fire plume. *Int. J. Wildland Fire,* **19,** 895–902.

——, and Coauthors, 2007: Observing the dynamics of wildland grass fires: FireFlux—A field validation experiment. *Bull. Amer. Meteor. Soc.,* **88,** 1369–1382.

——, S. Zhong, X. Bian, and W. E. Heilman, 2008: First observations of turbulence generated by grass fires. *J. Geophys. Res.,* **113,** D22102, doi:10.1029/2008JD010014.

Coen, J. L., 2005: Simulation of the Big Elk Fire using coupled atmosphere-fire modeling. *Int. J. Wildland Fire,* **14,** 49–59.

——, S. Mahalingham, and J. Daily, 2004: Infrared imagery of crown-fire dynamics during FROSTFIRE. *J. Appl. Meteor.,* **43,** 1241–1259.

Cunningham, P., 2007: Idealized numerical simulations of the interactions between buoyant plumes and density currents. *J. Atmos. Sci.,* **64,** 2105–2115.

——, S. L. Goodrick, M. Yousuff Hussaini, and R. R. Linn, 2005: Coherent vortical structures in numerical simulations of buoyant plumes from wildland fires. *Int. J. Wildland Fire,* **14,** 61–75.

Deardorff, J. W., 1974: Three-dimensional numerical study of turbulence in an entraining mixed layer. *Bound.-Layer Meteor.,* **7,** 199–226.

Goodrick, S. L., and D. E. Hanley, 2009: Florida wildfire activity and atmospheric teleconnections. *Int. J. Wildland Fire,* **18,** 476–482.

Grala, K., and W. H. Cook III, 2010: Spatial and temporal characteristics of wildfires in Mississippi, USA. *Int. J. Wildland Fire,* **19,** 14–28.

Haines, D. A., 1988: A lower atmospheric severity index for wild-land fires. *Natl. Wea. Dig.,* **13,** 23–27.

——, V. J. Johnson, and W. A. Main, 1975: Wildfire atlas of the northeastern and north central states. General Tech. Rep. NC-16, North Central Forest Experiment Station, USDA Forest Service, 25 pp.

Heilman, W. E., and X. Bian, 2008: Spatial and temporal evolution of atmospheric boundary-layer turbulence during the 1988 Yellowstone fires. *The '88 Fires: Yellowstone and Beyond,* R. E. Masters, K. E. M. Galley, and D. G. Despain, Eds., Tall Timbers Res. Station Miscellaneous Publ. 16, 21. [Available online at http://www.nps.gov/yell/naturescience/upload/'88fires.pdf.]

——, and ——, 2010: Turbulent kinetic energy during wildfires in the north central and north-eastern US. *Int. J. Wildland Fire,* **19,** 346–363.

Hinzman, L. D., M. Fukuda, D. V. Sandberg, F. S. Chapin III, and D. Dash, 2003: FROSTFIRE: An experimental approach to predicting the climate feedbacks from the changing boreal fire regime. *J. Geophys. Res.,* **108,** 8153, doi:10.1029/2001JD000415.

Inall, M., T. Rippeth, C. Griffiths, and P. Wiles, 2005: Evolution and distribution of TKE production and dissipation within stratified flow over topography. *Geophys. Res. Lett.,* **32,** L08607, doi:10.1029/2004GL022289.

Janjić, Z. I., 1994: The step-mountain Eta coordinate model: Further developments of the convection, viscous sublayer, and turbulence closure schemes. *Mon. Wea. Rev.,* **122,** 927–945.

Kanamitsu, M., W. Ebisuzaki, J. Woollen, S.-K. Yang, J. J. Hnilo, M. Fiorino, and G. L. Potter, 2002: NCEP-DOE AMIP-II Reanalysis (R-2). *Bull. Amer. Meteor. Soc.,* **83,** 1631–1643.

Linn, R., J. Winterkamp, C. Edminster, J. J. Colman, and W. S. Smith, 2007: Coupled influences of topography and wind on wildland fire behavior. *Int. J. Wildland Fire,* **16,** 183–195.

Lu, W., J. J. Charney, S. Zhong, X. Bian, and S. Liu, 2011: A North American regional reanalysis climatology of the Haines index. *Int. J. Wildland Fire,* **20,** 91–103.

Mellor, G. L., and T. Yamada, 1974: A hierarchy of turbulence closure models for planetary boundary layers. *J. Atmos. Sci.,* **31,** 1791–1806.

——, and ——, 1982: Development of a turbulence closure model for geophysical fluid problems. *Rev. Geophys. Space Phys.,* **20,** 851–875.

Mesinger, F., and Coauthors, 2006: North American Regional Reanalysis. *Bull. Amer. Meteor. Soc.,* **87,** 343–360.

Meyers, T. P., and D. B. Baldocchi, 1991: The budgets of turbulent kinetic energy and Reynolds stress within and above a deciduous forest. *Agric. For. Meteor.,* **53,** 207–222.

Morandini, F., X. Silvani, L. Rossi, P.-A. Santoni, A. Simeoni, J.-H. Balbi, J. L. Rossi, and T. Marcelli, 2006: Fire spread experiment across Mediterranean shrub: Influence of wind on flame front properties. *Fire Saf. J.,* **41,** 229–235.

Park, S.-B., J.-J. Baik, S. Raasch, and M. O. Letzel, 2012: A large-eddy simulation study of thermal effects on turbulent flow and dispersion in and above a street canyon. *J. Appl. Meteor.,* **51,** 829–841.

Potter, B. E., 2012a: Atmospheric interactions with wildland fire behaviour—I. Basic surface interactions, vertical profiles and synoptic structures. *Int. J. Wildland Fire,* **21,** 779–801.

——, 2012b: Atmospheric interactions with wildland fire behaviour—II. Plume and vortex dynamics. *Int. J. Wildland Fire,* **21,** 802–817.

Pryor, S. C., and Coauthors, 2009: Wind speed trends over the contiguous United States. *J. Geophys. Res.,* **114,** D14105, doi:10.1029/2008JD011416.

Rothermel, R. C., 1972: A mathematical model for predicting fire spread in wildland fuels. USDA Forest Service, Intermountain Research Station Research Paper INT-115, Ogden, UT, 41 pp.

Seinfeld, J. H., 1975: *Air Pollution: Physical and Chemical Fundamentals.* McGraw-Hill, Inc., 523 pp.

Sharples, J. J., R. H. D. McRae, and S. R. Wilkes, 2012: Wind–terrain effects on the propagation of wildfires in rugged terrain: Fire channeling. *Int. J. Wildland Fire,* **21,** 282–296.

Stull, R. B., 1988: *An Introduction to Boundary Layer Meteorology.* Kluwer Academic, 666 pp.

Sun, R., S. K. Krueger, M. A. Jenkins, M. A. Zulauf, and J. J. Charney, 2009: The importance of fire-atmosphere coupling and boundary-layer turbulence to wildfire spread. *Int. J. Wildland Fire,* **18,** 50–60.

Weigel, A. P., F. K. Chow, and M. W. Rotach, 2007: On the nature of turbulent kinetic energy in a steep and narrow Alpine valley. *Bound.-Layer Meteor.,* **123,** 177–199.

Werth, P. A., and Coauthors, 2011: Synthesis of knowledge of extreme fire behavior: Volume I for fire managers. General Tech. Rep. PNW-GTR-854, Portland, OR, U.S. Department of Agriculture, Forest Service, Pacific Northwest Research Station, 144 pp.

Westerling, A. L., A. Gershunov, T. J. Brown, D. R. Cayan, and M. D. Dettinger, 2003: Climate and wildfire in the western United States. *Bull. Amer. Meteor. Soc.,* **84,** 595–604.

Winkler, J. A., B. E. Potter, D. F. Wilhelm, R. P. Shadbolt, K. Piromsopa, and X. Bian, 2007: Climatological and statistical characteristics of the Haines index for North America. *Int. J. Wildland Fire,* **16,** 139–152.

Zulauf, M. A., 2001: Modeling the effects of boundary layer circulations generated by cumulus convection and leads on large-scale surface fluxes. Ph.D. dissertation, University of Utah, 177 pp.